ACS APPLIED NANO MATERIALS

www.acsanm.org Article

Cellulose Nanocrystal-Enabled Tailoring of the Interface in Carbon Nanotube- and Graphene Nanoplatelet-Carbon Fiber Polymer Composites: Implications for Structural Applications

Ozge Kaynan, Lisa M. Pérez, and Amir Asadi*

Cite This: *ACS Appl. Nano Mater.* 2022, 5, 1284−1295 Read Online

ACCESS | Metrics & More | Article Recommendations | Supporting Information

ABSTRACT: Cellulose nanocrystals (CNCs) enable the effective coating of carbon fibers (CFs) with pristine carbon nanotubes (CNTs) and graphene nanoplatelets (GnPs). Herein, we articulate the mechanisms that form the interface of CNC-bonded CNT and CNC-bonded GnP-CF reinforced polymer (CFRP) composites that are suitable for structural applications. We show that CNCs provide a suitable platform to engineer the interface of hybrid composites. We demonstrate that the hybrid nanomaterials, i.e., CNC and CNT/GnP, alter the chemical composition of the interface and its properties, and despite the similar elemental composition of the CNT and GnP, the mechanical properties of the produced composites differ. Our results show that the presence of CNC−CNT and CNC−GnP creates a 4 μm interfacial region that leads to a 200 and 145% increase in interfacial shear strength and a 46 and 28% enhancement in interlaminar shear strength, respectively. Furthermore, density functional theory calculations show that the binding energy between the CNC−CNT and CF sizing agent is 14% higher than that of CNC−GnP underlining the effect of chemical and physical interactions in the observed difference in mechanical properties. The understanding gained from this study highlights a path forward bottom-up manufacturing of hybrid composites with an engineered microstructure and properties from the molecular level and nanoscale to higher scales.

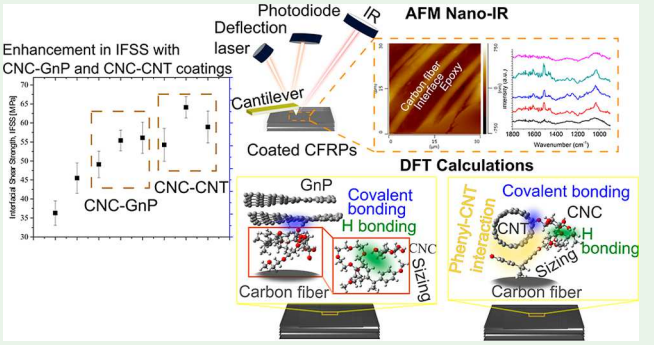

KEYWORDS: *cellulose nanocrystals, interface, carbon fiber reinforced polymer composites, carbon nanotubes, graphene nanoplatelet*

1. INTRODUCTION

A strong adhesion at the interfacial and interlaminar regions in carbon fiber (CF)-reinforced polymers (CFRPs) is key to maintaining an efficient load transfer between the fiber and matrix and enhancing interfacial properties,[1−6] interlaminar strength, and delamination resistance,[7−9] and final strength.[10] To achieve this, introducing nanomaterials (NMs) onto the surface of reinforcing fibers has been widely practiced to improve the interfacial properties of polymer composites.[11−14] The NMs are integrated onto the fiber surface by using several techniques including electrophoretic deposition,[2,8,13,15,16] dip/immersion coating on fibers,[11,17,18] dispersion in the sizing agent,[19,20] grafting the fiber surface,[3] and layer-by-layer assemblies.[21] Among these approaches, the dip/immersion coating is a simple and scalable technique, which enables the physical absorption of NMs on reinforcing fibers.[1,22]

To enhance the mechanical and functional properties of composites, carbon-based NMs such as carbon nanotubes (CNTs),[1−3,7,8,23−29] graphene nanoplates (GnPs)[3,7,8,20,30−33] and their combinations[12,22,34] have been widely used in CFRPs. Although the results of these studies serve well for their purpose, most of these processes rely on the chemical functionalization of CNTs and GnPs, which is an effective method, but it adds costs and causes damage to the CNT and GnP structure that deteriorates their intrinsic properties.[1,35] To lower the manufacturing costs of hybrid composites, it is ideal to use pristine CNTs and GnP; however, due to their strong Van der Waals attraction, homogeneous dispersion of pristine CNTs and GnPs is very challenging.[33]

In the last decade, cellulose NMs (CNs) have been increasingly used in applications such as manufacturing of composites with enhanced properties,[11,12,17,20] drug delivery,[36] electronics,[37] and polymer composites.[11,15,16,31,38−44] Being the most abundant polymer on the planet, CNs can be in the form of cellulose nanocrystals (CNC), cellulose nanofibrils/nanofibers (CNF), algae cellulose, and bacterial cellulose.[35] Among CN types, spindle-shaped CNCs (3−20 nm in width, 50−500 nm in length) possess high mechanical and thermal properties

Received: November 13, 2021
Accepted: January 3, 2022
Published: January 14, 2022

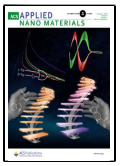

https://doi.org/10.1021/acsanm.1c03860
ACS Appl. Nano Mater. 2022, 5, 1284−1295

Scheme 1. Illustration of Hybrid CFRP Fabrication: (1) Preparation of Homogeneous CNC−CNT and CNC−GnP Suspensions by Probe Sonication Treatment, (2) Immersion Coating of CFs to Integrate CNC−CNT and CNC−GnP on CF Surface, and (3) Manufacturing of Coated CFs by VaRTM Method

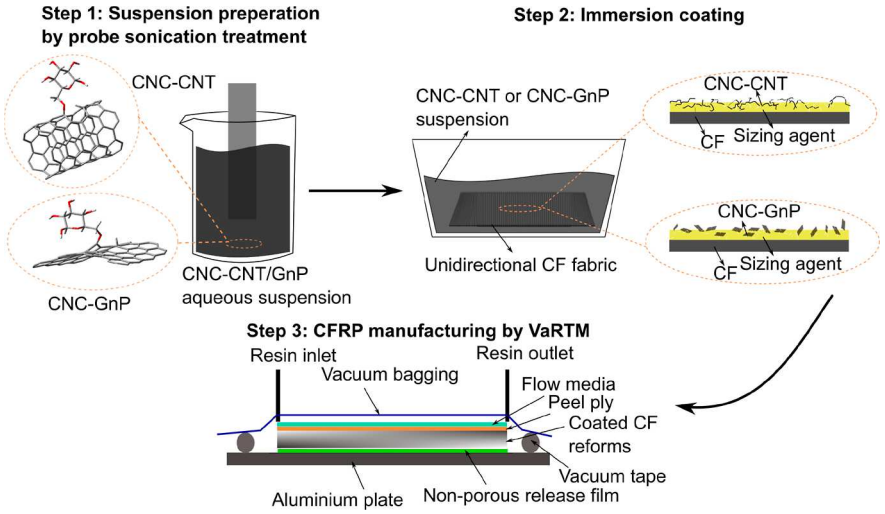

(∼5−7.5 GPa strength and ∼150 GPa modulus and stability up to 320 °C), low density (1.5 g/cm^3), and high aspect ratio (10−100), with abundant hydroxyl side groups (−OH), which can facilitate chemical/physical bonding with neighboring species.[35] The presence of abundant −OH groups and negatively charged sulfate half-ester groups (if hydrolyzed with the sulfuric acid) leads to the high colloidal stability of CNCs in water.[35,45−47]

There are many reports on integrating carbonaceous NMs,[2,7,16,22,42,48] CNs,[1,11] and their combinations[44] in fiber-reinforced polymer composites. Using hybrid carbonaceous NMs and CNs as a coating on the CF enables transferring their unique properties to CFRPs. This study attempts to unravel the underlying mechanisms behind the enhancement of the mechanical properties of CFRP composites for structural applications enhanced by hybrid CNCs and two different pristine carbonaceous NMs, i.e., CNT and GnP. CNCs are utilized to disperse and stabilize pristine CNTs and GnP in water without the need for any functionalization or dispersant. We then capitalize on understanding how CNC−CNT/GnP alters physical and chemical attributes of the interface and why the enhancement of mechanical properties differs for CNC−CNT- and CNC−GnP-coated CFRP composites. We probe the surface chemistry, morphology, and chemical composition of the interface at the nano- and micro-level and correlate them with macro-scale mechanical properties, such as tensile, flexural, and interlaminar shear strength (ILSS). Moreover, we employ density functional theory (DFT) calculations to capture the interactions of CNC−CNT and CNC−GnP with the sizing agent of the CF to unravel the effect of the geometry and morphology of hybrid NMs on the formation of the microstructure at the interface.

2. MATERIALS AND METHODS

2.1. Materials. Unidirectional (UD) Hexcel IM2 CFs (12 k tow size) are used as received. Epoxy INF-114 and INF-211 hardeners are supplied from Pro Set (USA). NCV-100 CNCs (CelluForce, Canada) with a diameter of 2.3−4.5 nm and length of 44−108 nm are used as received. Pristine multi-walled CNTs produced via catalytic CVD with 95% carbon purity and average outer and inner diameters of 5−15 nm and 3−5 nm and length of ∼10 μm are purchased from USNano (USA). GnPs (EG016) are supplied from Celtig (USA) with 2−5 μm dimensions measured by scanning electron microscopy (SEM).

2.2. Fabrication CNC−CNT/GnP-Coated CFRP. Three coating suspensions with a concentration of 0.2 wt % including CNC, CNC−CNT 4:1, 6:1, 8:1, 10:1, and 12:1, and CNC−GnP 1:1, 2:1, 4:1, and 6:1 are dispersed in deionized water using probe sonication (Qsonica Q125 and a sonotrode of 6 mm) at a frequency of 20 kHz and 75% intensity in an ice bath, as illustrated in Scheme 1. The corresponding labeling scheme used to describe the coated CFs and hybrid composites is CNC−CNT and CNC−GnP *m:n*, where *m* and *n* represent the mass ratio of CNC and CNT/GnP, respectively, in the coating suspension. The wording "hybrid composites" in this study represent that one substance was integrated as a reinforcing material, that is, CNCs and CNT/GnP along with the CFs of the CFRPs, in which a new NM structure/system with new features of the combination of cellulose (dispersibility due to their hydroxyl groups) and carbonaceous NMs (stiffness for reinforcing role) is created.

Dry UD 12 in × 12 in CF fabrics are separately immersed in a bath filled with the prepared aqueous suspensions and left for 20 min at room temperature (Scheme 1). Then, the coated CFs are dried overnight followed by drying in an oven at 120 °C for 12 h.

The hybrid composites are manufactured using coated CF layers with a $[0_2,90_2,0_2]_s$ stacking sequence via a vacuum-assisted resin transfer molding (VaRTM) process (Scheme 1) described in detail in our previous work.[48] Short beam, flexural and tensile samples are cut from the fabricated plates using a waterjet (Jet Edge waterjet systems X-5, Minnesota, USA).

2.3. Characterization and Testing. To evaluate the dispersion stability, ζ-potential of 0.2 wt % CNC, CNC−CNT 4:1−12:1, and CNC−GnP 1:1−6:1 in water is measured at room temperature in a Malvern Zeta-sizer Nano ZS. An average of at least five measurements is reported.

The interfacial properties of CFRPs are measured using in-situ single fiber fragmentation (SFF) tests in a Kammrath Weiss 10 kN micro tensile stage under an optical microscope (DXS 500 by Olympus). The SFF specimens are prepared by embedding a single filament extracted from a coated CF tow into the dog-bone-shaped silicone mold filled with an epoxy resin and cured. The dog-bone shape samples are 50 × 10 mm with a gauge length of 25 mm, as shown in Figure S1. The interfacial shear strength (IFSS) values are calculated by the Kelly and Tyson[49] model in eq 1

$$\tau = \frac{d_f \sigma_f}{2 l_c} \quad (1)$$

https://doi.org/10.1021/acsanm.1c03860
ACS Appl. Nano Mater. 2022, 5, 1284−1295

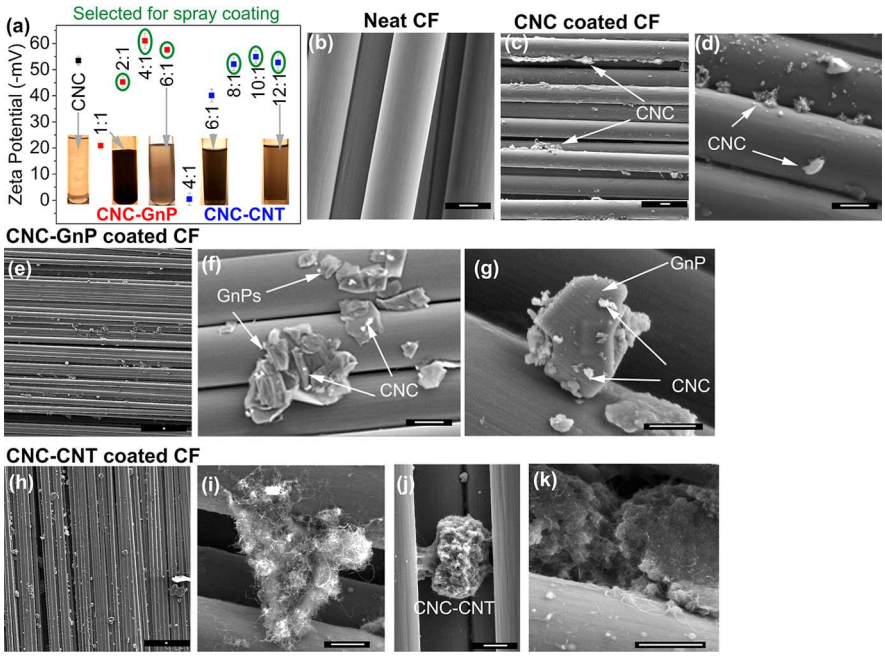

Figure 1. (a) Dispersion state vial photographs and ζ-potential of CNC, CNC−GnP, and CNC−CNT suspensions. Green circles show the selected CNC−CNT/GnP for coating and CFRP manufacturing. SEM images are shown in (b) neat CF, (c,d) CNC-coated CF, (e−g) CNC−GnP-coated CF, and (h−k) CNC−CNT-coated CF. The white scale bar in the black box is 2 μm.

where τ is IFSS, d_f is the fiber diameter, l_c is the critical length, and σ_f is the fiber tensile strength at critical length. The critical length, l_c, is calculated by $l_c = 4/3\bar{l}$, where $\bar{l}$ is the average fiber length. The video in the Supporting Information was taken during the SFF under an optical microscope, and an average of 6 samples is reported. Weibull distribution used for the CF strength data (according to ASTM D3822) is applied to obtain Weibull shape parameter and strength as 4.91 and 4038 MPa, respectively. Note that the individual fibers are pulled out from the NM-coated fabric. Batista et al.[11] compared the coated 12 k CF tow with an individual CF and reported that the IFSS results did not change significantly.

X-ray photoelectron spectroscopy (XPS) is used to quantitatively analyze the chemical groups on the CNC, CNC−CNT, and CNC−GnP coated CFs. 5 × 5 mm CF samples are analyzed by a monochromatic Mg K (*hv*: 1256.6) X-ray source of 300 W operating at 15 kV in XPS (Omicron XPS/UPS system with Argus detector). Peak analysis and quantitative elemental composition are performed using CasaXPS software, where the peaks are shifted to 284.8 eV (C−C/C═C bond) and 532.0 eV (O═C bond) in C 1s and O 1s, respectively. Before the XPS analysis, all samples are conditioned in a vacuum oven for 12 h to eliminate outgassing.

To visualize the quality of the NM-coated CF surface, SEM (Tescan FERA-3 Model GMH Focused Ion Beam Microscope) with an acceleration of 10 kV is used with the same sample dimensions as in XPS.

The atomic force microscopy (AFM) nano-IR (Bruker Anasys nano-IR2) is conducted to understand the topological and chemical evolution at the CF/epoxy interface with the addition of NMs. AFM-nano-IR simultaneously probes both topology (AFM) and evolution of the chemical composition of the interface (IR) of CFRP composites. The specimens are prepared by inserting and taping a CF tow on the top of a silicone holder 2 × 5 × 1 cm poured with epoxy. To obtain a smooth surface, CFRP is ground using 400−7000 grit sandpapers and polished with aluminum nanoparticles of 6 μm size. The AFM micrographs are collected at the AFM tapping mode and taken from the top view, and the measurements are conducted for at least 3 samples for each composite. The IR measurements are performed in the range of 1800−800 cm^{-1} with 20 nm spatial resolution. All nano-IR spectra are obtained with 200 cm^{-1} 1/s scanning speed at a resolution of 2 cm^{-1}.

The short beam shear test is performed according to ASTM D2344 standard to report ILSS of neat and coated CFRPs. At least seven rectangular specimens of 25 × 6 × 3 mm are tested under three-point bending at a cross-head speed of 1 mm/min until a deflection equal to the thickness of the specimen was achieved.

For the flexural strength, three-point bending tests are conducted according to ASTM D790 on specimens with the dimensions of 120 × 12.7 × 1.5−2 mm and in the span to depth ratio of 40:1. The crosshead speed is adopted as 3 mm/min. The tensile strength is measured according to ASTM D3039 with dimensions of 165 mm length, the width of 13 mm, the gauge length of 50 mm, and the thickness of 2.5 mm. The crosshead speed is 5 mm/min.

2.4. DFT Calculations. Although the experiments report the effects of CF coating on the interfacial and mechanical properties, DFT calculations are used to reveal the interactions of NMs with CFs and the mechanism behind the enhancement of interfacial properties. DFT calculations are performed using the Gaussian 16 suite of programs at Texas A&M high-performance research computing. The B3LYP-GD3BJ functional[50] with Pople style 6-31G(d′,p′)[51] double-ζ quality basis was used. The SMD implicit solvation model[52] is used to include the bulk interaction of the solvent with dissolved molecules. CNCs added to the single vacancy (sv)-defected sites of arm-chair single-walled CNT and GnP NM model systems with a sv, as observed in Figure S2, were computed and the binding energy between the NMs and the model sizing agent of CF were calculated. As the sizing of Hexcel IM2 is proprietary data, we used a known CF sizing agent [hydrophobic bisphenyl A and hydrophilic polyethylene glycol (PEG)] available from the literature and compatible with epoxy[53] (see Figure S3).

3. RESULTS AND DISCUSSION

3.1. Dispersion Quality of CNC−CNT/GnP and Coated CFs. The agglomerate-free NM coating on CFs is essential to enhance the interfacial and macroscopic properties.[12] CNCs are hydrophilic nano-spindles dispersed in aqueous media with colloidal stability as their negative sulfate groups create electrostatic repulsion. We show that the CNC is able to disperse and stabilize highly hydrophobic pristine CNTs and GnPs in water. Figure 1a displays the photographs of stable

https://doi.org/10.1021/acsanm.1c03860
ACS Appl. Nano Mater. 2022, 5, 1284−1295

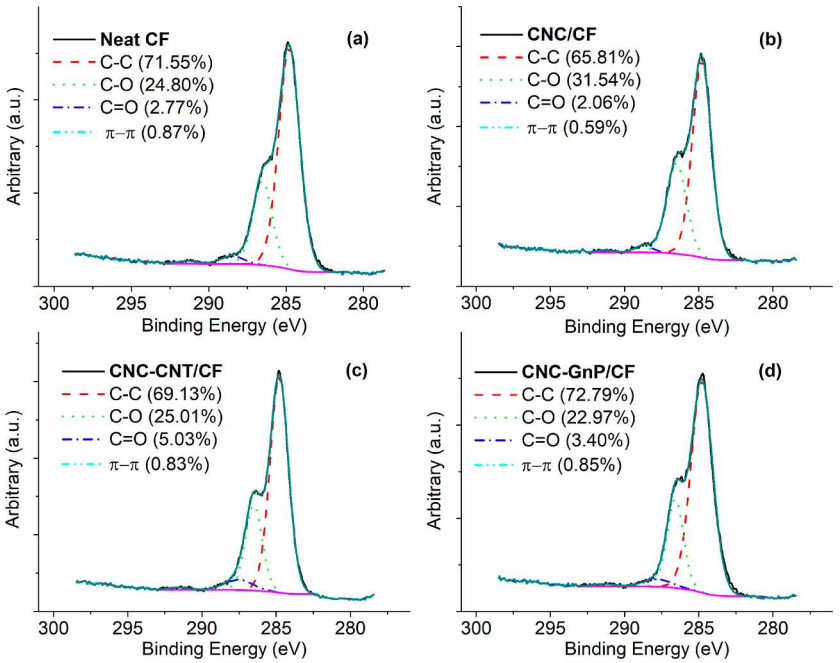

Figure 2. XPS analysis of (a) neat CF, (b) CNC-coated, (c) CNC−CNT-coated, and (d) CNC−GnP-coated CF.

dispersions of CNC, CNC−GnP, and CNC−CNT hybrids and their ζ-potential values. Transparent suspension of CNCs without any agglomeration is a visual indication of a good dispersion state. By the incorporation of CNTs/GnPs into the CNC aqueous suspension, the color is changed to grey/black. The increase of the CNC ratio in CNT/GnP suspension leads to a more transparent suspension [both CNC−CNT (12:1) and CNC−GnP (8:1)] without any visual sign of agglomeration.

To further examine the dispersion quality of CNC−CNT/GnP, ζ-potential (Figure 1a) is conducted for different mass fractions of hybrid NMs. The ζ-potential values of the CNC−GnP suspensions increase gradually with the addition of CNCs, which are 20, 45, 61, and 58 mV for CNC−GnP 1:1, 2:1, 4:1, and 6:1, respectively. These values are in the order of ζ-potential of CNCs (53.5 mV), implying the effectiveness of CNCs in dispersing GnPs in water. Moreover, the ζ-potential of CNC−CNT 4:1, 6:1, 8:1, 10:1, and 12:1 is measured as ∼0, 40, 52, 54, and 53 mV, respectively, indicating that CNCs assist in detaching CNTs as well as enhancing the colloidal stability. The mass ratios of 8:1, 10:1, and 12:1 CNC−CNT and 2:1, 4:1, and 6:1 CNC−GnP are used in the coating process and CFRP manufacturing, which are selected according to the highest ζ-potential values (Figure 1a). Overall, these results suggest that CNCs successfully disperse hydrophobic pristine CNTs and GnPs in water without using any additives because of (i) the presence of strong negatively charged surfaces of sulfonated CNCs that stabilize CNCs in water, (ii) electrostatic repulsion and stabilization with the higher surface charge of CNCs,[54] and (iii) strong interactions between CNCs and carbonaceous NMs.[55] Our experiments indicate that CNCs can overcome the strong Van der Waals interaction between CNTs (or GnPs) and act as a stabilizer for them in aqueous media.

ζ-Potential values of CNC−GnP and CNC−CNT suspensions range between 45−61 and 40−54 mV, respectively. A similar ζ-potential value allows balancing the cost-performance of the suspension. CNTs/GnPs can be dispersed even at low CNC concentrations i.e., CNC−GnP 2:1 and CNC−CNT 6:1 lead to the reduction in the amount of material used and cost. This also enables the control of the interfacial properties. The interactions between the CF and epoxy are enhanced with integrated high concentration CNCs, whereas mechanical and electrical conductivity properties can be tailored by introducing a high amount of CNTs/GnPs. Hence, these materials are suitable not only for reinforcing CFRPs but also for surface coating applications such as thin films.

SEM images of neat CF (Figure 1b), CNC (Figure 1c,d), CNC−GnP (Figure 1e−g), and CNC−CNT (Figure 1h−k)-coated CFs are displayed to ensure that NMs are successfully transferred onto CFs by the immersion coating process. Compared to the neat CF surface (Figure 1b), the deposition of CNCs increases the surface roughness of the CFs (Figure 1c,d). A similar trend is observed in the CNC−GnP-coated CF surface (Figure 1e). Closer examinations of CNC−GnP coating display that the GnP layers are attached to the CF surface from their largest surfaces (Figure 1f), and CNCs are attached to the surface of micron size GnP (Figure 1g). Similar to CNC−GnP (Figure 1e), the CNC−CNT deposition increases the surface roughness of CFs, as shown in Figure 1h. The hybrid CNC−CNT acts as a binder between CFs (Figure 1i−k), where CNC−CNTs are entangled and create an intertwined network. Yet, no entanglement is observed in CNC−GnP-coated CFs as the CNCs attach to the GnP surface individually or in small clusters (Figure 1g). From these experiments, it is concluded that CF surfaces are effectively coated with hybrid CNC−CNT/GnP through a facile and simple immersion coating process without the use of chemicals or additives.

3.2. Surface Chemistry of CNC−CNT/GnP-Coated CFs.

XPS analysis (C 1s peaks) is conducted to analyze the effect of hybrid NMs on the chemical groups created on the CF surface by the immersion coating process (Figure 2 and Table S1). The surface modification results in changing the surface chemical properties and relative amount of C 1s components. These are mainly manifested by the types and contents of the

https://doi.org/10.1021/acsanm.1c03860
ACS Appl. Nano Mater. 2022, 5, 1284−1295

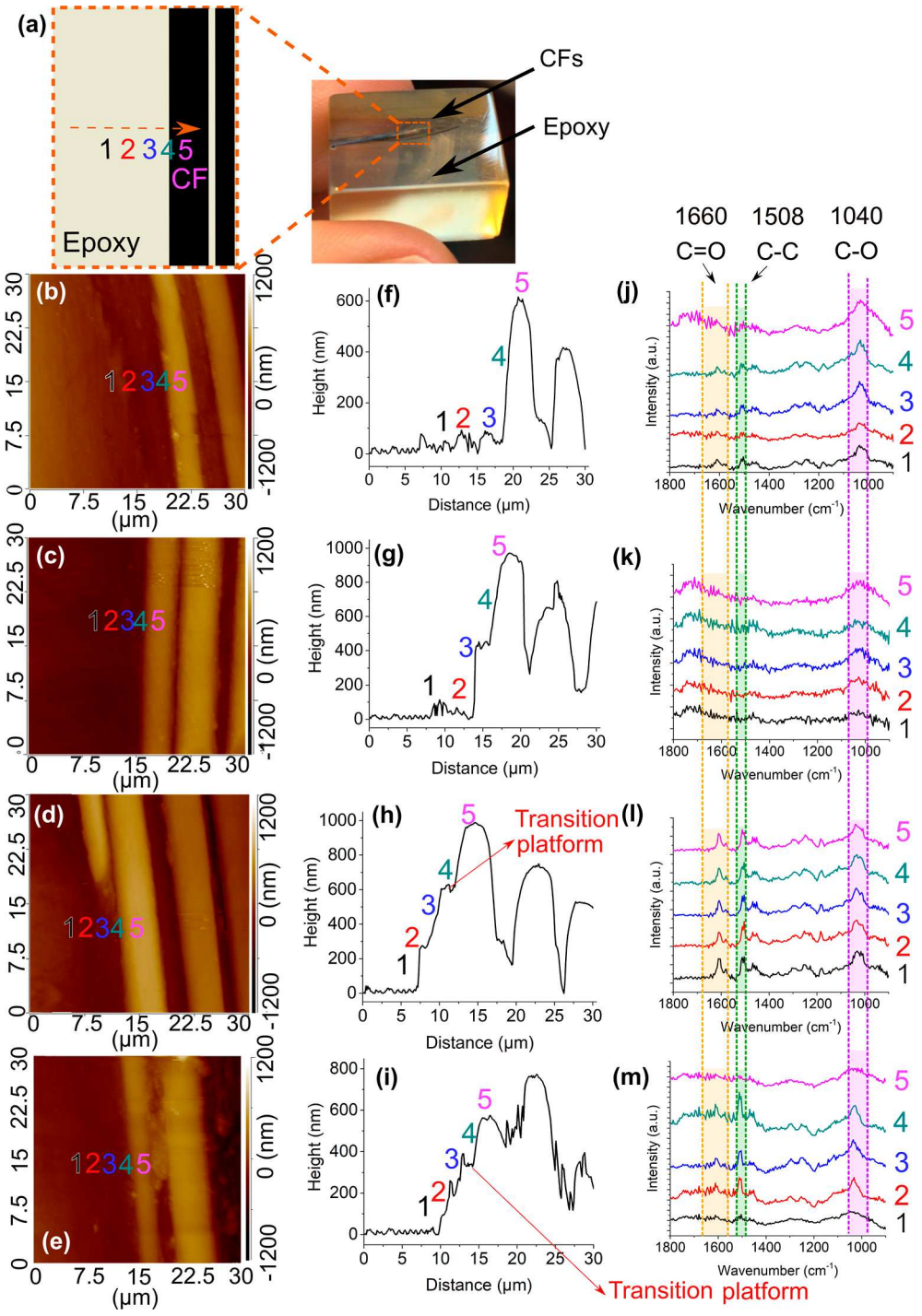

Figure 3. AFM-nano IR analysis of neat CF, CNC-coated, CNC−GnP 4:1-coated, and CNC−CNT 10:1-coated CFRPs. (a) The schematic of procedure and selected 5 points and the sample. The AFM micrographs of (b) neat CF, (c) CNC-coated, (d) CNC−GnP 4:1-coated, and (e) CNC−CNT 10:1-coated CFRP for an area of 30 × 30 μm and (f−i) the corresponding height-lateral plots showing height variation from epoxy to CF regions (from points 1−5) and the interface in between. The color scale of dark brown to beige presents the height difference (dark brown is the lowest and beige is the highest). (j−m) IR spectra are in the range of 1800−900 cm^{-1} with highlighted peaks at C═O (1660 cm^{-1}), C−C (1508 cm^{-1}), and C−O (1040 cm^{-1}).

active groups such as the oxygen-containing group on the CF surface[13] that enhances the chemical affinity of CFs with the polymer matrix.[1,2,11,12]

The neat CF has four peaks C−C (71.55%), C−O (24.80%), C═O (2.77%), and $\pi-\pi$ (0.87%) (Figure 2a). With the deposition of CNCs with abundant −OH groups, the relative amount of C−O increases to 31.54% while the C═O content remains unchanged (Figure 2b). Also, the increase in oxygen-containing groups confirms that CNCs are successfully transferred on the CF surface[56] during the immersion coating process. Having polar oxygen-containing groups on the CF surface is crucial for creating potential sites for physical and chemical bonding with epoxy during curing. This contributes to achieving strong interfacial interactions between the CF and

https://doi.org/10.1021/acsanm.1c03860
ACS Appl. Nano Mater. 2022, 5, 1284−1295

the bulk epoxy matrix. Figure 2c shows that on the CNC−CNT-coated CF surface, both oxygen-containing groups, i.e., C−O and C═O, increase by 5 and 100%, respectively, compared to that of neat CF. This indicates that CNC−CNT coating contributes to the chemical attributes of the CF surface. For CNC−GnP-coated CF (Figure 2d), the C═O increases by 23% and C−O remains constant compared to neat CF. This also indicates that the addition of CNC−GnP promotes C═O groups attached on the CF surface as a chemically active group to enhance interfacial adhesion.[13] The contribution of $\pi-\pi$ bonding is very weak and ranges from 0.59 to 0.87%, which is related to the interactions between sizing molecules (phenyl groups) and carbonaceous NMs. Overall, XPS results reveal that CNCs not only act as a dispersing agent in water to form a homogeneous coating suspension but also provide chemically active components on the surface of the CF that can increase the adhesion of the carbonaceous NMs to the CF and potentially increase the wettability of the fibers with epoxy during manufacturing.[12]

3.3. Interfacial Region (Interphase) Characteristics of CNC−CNT/GnP-Coated CFRPs. The chemical composition and topology of the modified CFRP interface with different coatings are studied by AFM nano-IR (Figure 3). IR spectroscopy is commonly used to investigate the chemical composition and structure of materials. However, because its spatial resolution is at several micrometers, it is difficult to capture the variation of chemical composition at the interface. On the other hand, the AFM-Nano IR technique has enabled IR analyses with a spatial resolution of 20 nm or higher, thus making it a powerful tool for studying the chemical composition of the interface at a nanoscale resolution for adhesion studies.[57] Herein, to investigate the variation of the chemical composition at the interfacial region, five distinct points (1−5) from epoxy to the CF with a 2 μm distance are selected on the interfacial region of CFRP, on which the IR spectra are collected (see Figure 3a).

The thickness of the CFRP interphase plays an important role in creating an efficient stress transfer from epoxy to the CF that defines the overall composite properties. The thickness of the interfacial zone (interphase) increases with the addition of NMs.[58] This can be attributed due to the presence of functional groups that bind to the polymer matrix as well as the increased mechanical interlocking of the CF with epoxy because of protruded NMs.[5] Figure 3 also displays the AFM micrographs of neat CF (Figure 3b), CNC-coated (Figure 3c), CNC−GnP 4:1-coated (Figure 3d), and CNC−CNT 10:1-coated (Figure 3e) CFRP with five distinct points from epoxy (point 1) to CF (point 5), the corresponding lateral height versus distance (Figure 3f−i), and IR spectra (Figure 3j−m). In the neat CFRP (Figure 3b), a sudden rise from ∼0 to ∼600 nm occurs between points 3−5, as depicted in the AFM height-distance plot in Figure 3f. This indicates the presence of a minimal gradual transition at the interface. Yao et al.[59] showed that the span of the interface in neat CFRP composites is 210 nm using AFM force modulation images and stiffness distribution. In contrast, for CNC−CFRP (Figure 3c), there is a relatively a gradual change from point 2 (0 nm) to point 3 (400 nm) and point 4 (600 nm) before rising to 1000 nm at point 5 (CF surface) (Figure 3g). This indicates that a ∼2 μm gradient interfacial region (interphase) is formed in CNC−CFRP composites. The gradient interface becomes more pronounced in CNC−GnP-coated CFRP. The AFM image (Figure 3d) and height-distance plot (Figure 3h) show that ground point 1 locates around 0 nm. The height gradually rises from point 1 to point 2 (250 nm), point 3 (450 nm), and point 4 (650 nm), referred to as an interfacial region, and finally reaches point 5 (CF surface) at 950 nm (Figure 3h). The measurements reveal that there is a 4 μm interfacial region in CNC−GnP-coated CFRP. A similar trend is observed in CNC−CNT-coated CFRP (Figure 3e), where the height plot (Figure 3i) jumps from 0 (point 1) to 100 nm (point 2), ∼300 nm (point 3), 400 nm (point 4), and finally 600 nm at point 5. Herein, the interfacial region for CNC−CNT-coated CFRP around is also measured as 4 μm. The size of the interface is in accordance with other research works.[16,58,60] Srivastava et al.[58] reported that GnP deposition onto CFs results in the formation of an interface up to 3 μm revealed by energy-dispersive system linear scanning. The created 4 μm interface in this study is possibly the contribution of a hybrid CNC−CNT/GnP material system. In conclusion, the stiffened and broadened interfaces at CNC−CNT/GnP relieve the stress concentration that facilitates a smoother stress transfer from the matrix to fiber, which is essential to enhance the interfacial properties of CF and epoxy.

The transition layer in CNC and CNC−CNT/GnP-coated composites indicates that NMs enhance the fiber-resin connection and mechanical engagement at the interface region, which was also seen in amide acid/silicon oxide,[61] CNTs,[62,63] OCNTs,[64] and graphene[65]-reinforced CFRPs. The interfacial transition layer theory indicates that the interface load transfer capacity can be significantly enhanced by a transition layer between the reinforcing material and the matrix.[66] The platform-like transition at point 4 (Figure 3h,i), where the sizing agent interacts with the NMs, in CNC−GnP and CNC−CNT-coated composites indicates the improved molecular compatibility of the sizing agent and epoxy. A similar trend was also reported in amide acid/silicon oxide[61] and TEMPO-modified CNC[67]-reinforced composites. This suggests that the interactions of the sizing agent and NMs play an important role in the formation of the transition layer.

IR spectra between 1800 and 900 cm^{-1} are presented in Figure 3j−m, and the IR peaks at 1660 cm^{-1} (C═O), 1508 cm^{-1} (C−C), and 1040 cm^{-1} (C−O) are investigated to reveal the interaction between epoxy and the NM-coated CF. Stretches in the aromatic ring (C−C peak) at points 3 and 4 indicate the interactions of CFs with the epoxy. The intensity of C═O and C−O groups of neat CFRP (Figure 3j) slightly increases when approaching the CF (from points 1−4), which might be the contribution of the sizing layer of CFs. In contrast, CNC coating (Figure 3k) increases the relative C−O peak especially at the interface region (between points 3 and 4) and the CF surface (point 5). This implies that CNC interacts with both hydrophilic sizing PEG and the epoxy. The abundant −OH group in the cellulose structure[35] leads to creating a peak at C−O stretching at 1040 cm^{-1}, which is also confirmed in Figure 2b. In CNC−GnP-coated CFRP (Figure 3l), the C−C peak relatively increases at points 3 and 4. Also, the CNC−GnP coating leads to a slight increase of C−O and C═O peaks at the interface between points 2 and 4 (Figure 3l). Similarly, in CNC−CNT-coated CFRP (Figure 3m), C−O and C═O peaks are dominant at points 2, 3, and 4, suggesting the formation of stronger bonds at the interface possibly due to the synergistic effect of hybrid NMs that enhances the interactions with epoxy and CFs. The increase in the C−C peak at points 2, 3, and 4 is distinct, which indicates the enhanced interactions of epoxy and CF as a result of the

https://doi.org/10.1021/acsanm.1c03860
ACS Appl. Nano Mater. 2022, 5, 1284−1295

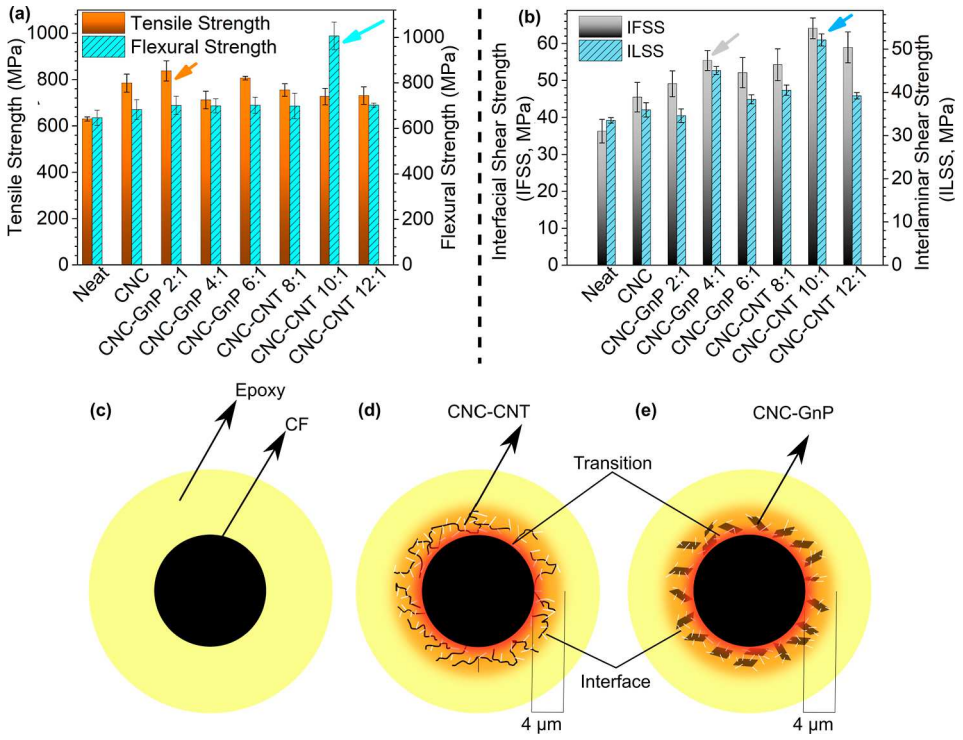

Figure 4. (a) Tensile and flexural strengths and (b) IFSS and ILSS of neat, CNC, CNC−GnP, and CNC−CNT-coated CFRPs. The arrows indicate the best ratio of CNC−CNT/GnP according to the mechanical properties. The reinforcing mechanism of (c) neat, (d) CNC−CNT, and (e) CNC−GnP-coated CFRPs.

CNC−CNT coating. Moreover, they also correlate with the 4 μm interfacial region in AFM images where the gradual transition is observed between points 2 to 4. Overall, both CNC−CNT and CNC−GnP-coated CFRP increase polar bonding (C−O and C═O) at the interface region along with the gradual interface formation, indicating the formation of strong interfacial adhesion in CF and epoxy.

3.4. Mechanical Properties of CNC−CNT- and CNC−GnP−CFRPs. The mechanical properties of CNC, CNC−CNT, and CNC−GnP-coated CFRP composites are evaluated by flexural and tensile strengths, as shown in Figure 4a. The mass fractions of CNC−GnP (2:1, 4:1, and 6:1) and CNC−CNT (8:1, 10:1, and 12:1)-coated CFRPs are selected based on the highest ζ-potential (Figure 1a) and agglomerate free state of suspensions. Integrating NMs at the interface of CFRP contributes to the flexural strength of CNC, CNC−CNT, and CNC−GnP-coated CFRPs. CNC coating increases the tensile strength by 23% compared to that of neat CFRP. This enhancement is attributed to the abundant polar groups (Figure 2b), leading to stronger physical binding and covalent bonding with epoxy.[10,68] The most dominant enhancement is achieved in CNC−CNT 10:1 coated CFRP, on which the flexural strength increases by 55% compared to those of neat CFRP. Also, note that this enhancement is ∼48 and 42% higher than those of CNC and CNC−GnP 2:1 coated CFRPs, respectively. As the flexural properties are related to a combination of in-plane and out-of-plane performance of composites, this improvement is attributed to the synergistic effect of hybrid CNC−CNT that enhances both interfacial and interlaminar properties of CFRP. Interestingly, although both CNC−GnP and CNC−CNT enhance the tensile strength of the composites, CNC−GnP improves the tensile strength higher than that of CNC−CNT. This is especially observed in CNC−GnP 2:1 and CNC−GnP 6:1-coated CFRPs with 33 and 28% higher tensile strength in comparison to neat CFRP, respectively, whereas the contribution of CNC−CNT integration ranges between 15 and 19% for CNC−CNT 8:1 and 12:1, respectively. These results imply that CNC−CNT improves the combined in-plane and out-of-plane (flexural strength) properties of CFRP better, whereas CNC−GnP enhances the in-plane properties (tensile strength) more effectively. The potential reason might be attributed to the geometry, morphology, and molecular interactions of CNC−GnP-coated and CNC−CNT-coated CFs, in which the nanosheet-shaped GnPs prefer to be aligned with the CF orientation in the in-plane direction (see SEM images Figure 1e−g), whereas tube-shape CNTs create an intertwined network in-plane and out-of-plane directions (Figure 1h−k).

The mechanical performance of CFRPs is closely related to the interlaminar and interfacial properties.[2,19,63] Integrating CNC−GnP 4:1 and CNC−CNT 10:1 increases the ILSS by 28 and 46%, respectively, compared to those of neat CFRP (35.52 MPa) (Figure 4b). The interfacial properties of neat and NM-coated CFRPs are also presented in Figure 4b. Overall, the integration of CNC, CNC−GnP, and CNC−CNT in CFRPs enhances the IFSS. The maximum IFSS enhancement is noted in CNC−GnP 4:1 and CNC−CNT 10:1 with 145 and 200%, respectively. The nano-scale improvement modifies the mesoscale properties of the CFRP interface, and this enhances the macro-scale properties such as tensile and flexural strength. There is a linear correlation between bulk properties and IFSS and ILSS. This can be attributed to the CNC−CNT/GnP suspensions successfully penetrating the CF tows and creating physical and chemical bonds with CF and epoxy.

https://doi.org/10.1021/acsanm.1c03860
ACS Appl. Nano Mater. 2022, 5, 1284−1295

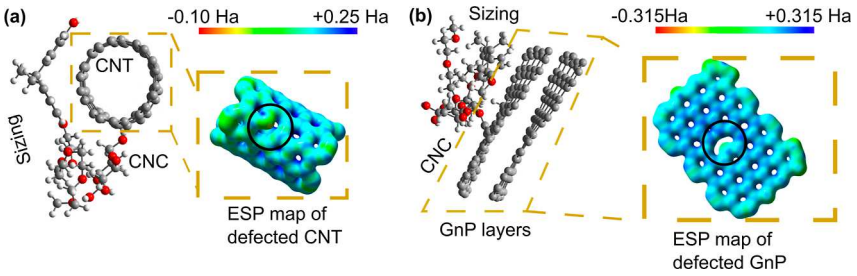

Figure 5. ESP maps of (a) svCNT and (b) svGnP with the black circles indicate that the unoccupied orbital has high electropositivity (dark blue). The iso-value is 0.04.

The formation and size of the interfacial region play a key role in the interfacial properties of CFRPs. The gradient and smooth change in the interphase facilitates the efficient stress transfer from epoxy to CF. The largest enhancement in IFSS is achieved in CNC−CNT 10:1 and CNC−GnP 4:1-coated CFRP (Figure 4b), which is attributed to the enlarged interfacial span (4 μm) compared to that of CNC-coated CFRP (2 μm) and neat CFRP (∼0) (Figure 3). Moreover, the stiff and high aspect ratio of CNTs and GnPs act as a binder at the interface that results in a stronger interface with improved damage resistivity.[12,62] The proposed reinforcing mechanism is sketched in Figure 4c−e. The interface region of neat CFRP cannot be captured in AFM-nano IR analysis (Figure 4c). In contrast, integrating CNC−CNT/GnP (Figure 4d,e) creates a 4 μm interfacial region as a result of a hybrid NM system. Also, a platform-like transition layer at the interface indicates enhanced interactions with the sizing agent and the epoxy due to the presence of NMs. In conclusion, broadened interfaces at CNC−CNT/GnP facilitate a smoother stress transfer from the matrix to fiber.

Overall, the improvement in IFSS can also be attributed to the synergy between several mechanisms including (i) increase of the wettability of reinforcing fiber with epoxy due to the presence of abundant −OH groups from CNCs,[20,67] (ii) increase of the surface roughness of CFs by the coating that leads to mechanical interlocking,[1,11,66,67] (iii) physical and chemical bonding between CF-NMs-epoxy,[12,66] and (iv) uniform dispersion and distribution of NMs and stability of the coating suspensions. The introduction of the −OH group via CNCs makes the CF surface attractive for chemical bonds to the epoxy and CF sizing agent. As expected, the trend in IFSS is similar to that of ILSS properties because of the dual reinforcing phenomena, that is, oxygen-based functional groups (CNC) and mechanical interlocking (CNT/GnP) at the interface that promote ILSS. Despite the increase of IFSS and ILSS in both CNC−CNT/GnP coated CFRPs, Figure 4b shows that the IFSS and ILSS values of CNC−CNT-coated CFRP are higher than that of CNC−GnP.

Our results show that CNC−CNT/GnP coating enhances the IFSS, ILSS, flexural and tensile strength. Despite the similar size order (∼5−10 μm) and NM content in coating suspension (0.2 wt %) as well as similar interfacial region size (4 μm, see Figure 3) for both CNC−CNT and CNC−GnP-coated CFRP, the enhancement of IFSS, ILSS, and mechanical strength is dissimilar. This can be due to the difference in surface chemistry and at the interface dictated by CNC−CNT and CNC−GnP, as shown in Figures 2 and 3. To probe the underlying mechanisms, we conducted quantum level calculations to understand how GnP and CNT contribute to the formation of the interfacial region and its chemical composition/bonding.

3.5. DFT Calculations. We implement quantum level DFT calculations to investigate the interactions between the hybrid NMs and the CF surface/sizing layer and to understand the platform-like transition reported in AFM-nano IR (Figure 3). DFT calculations are to test the potential binding between CNC and CNT/GnP as well as the effect of the difference in geometry and morphology CNC−CNT and CNC−GnP (i.e., nanotube and nanosheet structures) on binding energies, which might influence the mechanical properties, IFSS, and ILSS of CNC−CNT- and CNC−GnP-coated CFRPs.

Particle−particle interaction in hybrid systems affects the interfacial properties that define the mechanical performance of composites. Hence, the formation of strong bonding between CNC and CNT/GnP is crucial for enhancing the interfacial properties of CFRPs. Shishehbor and Pouranian[69] reported the importance of non-bonding interactions between CNC and CNT on adhesion energy (or binding energy), in which the effect of the thickness of CNC layers wrapped on the CNT under various loading conditions was articulated by MD simulations. It was shown that the rise in cellulose content increased the adhesion energy of CNT-wrapped CNCs almost 2-fold due to the hydrogen bonding.[69,70] Along with the non-bonding interaction between CNC−CNT/GnP, covalent bonding formation may occur through the defected sites of carbon structures. The carbonaceous NMs, i.e., CNTs and GnPs are synthesized with inherent manufacturing defects including single vacancy (sv), double vacancy (dv), and Stone Wales (sw).[71] The sv is one of the most common carbon defect types[72] which contains one unsaturated carbon that makes it more reactive than the other type of defects. Therefore, in this study, the sv type of the carbon defects is used in CNT and GnP models (Figure S2). Figure 5 displays highly reactive sv defected sites of the CNT and GnP in the electrostatic potential (EPS) maps. The absence of a carbon atom results in highly electropositive sites on the CNT/GnP structure, where hydroxyl groups of CNCs replace water molecules and covalently bond (C−O) to the defected sites. We hypothesize that the energy barrier of this covalent bonding is overcome during ultrasonic treatment. Therefore, the bonding between CNC and CNT/GnP is not merely a physical interaction and rather primary bonds, that is, covalent bonding also exists. In our DFT calculations, we use hybrid nanostructures, i.e., CNC−CNT and CNC−GnP, in which CNCs are covalently bonded to CNTs/GnPs from their sv-defected sites. To omit the size effect, the CNT is constructed as 10 Å long and 7 Å diameter and GnP as 10 × 15 Å with the chirality of $n = m = 5$, as shown in Figure 5a,b, respectively.

https://doi.org/10.1021/acsanm.1c03860
ACS Appl. Nano Mater. 2022, 5, 1284−1295

The chemical interactions of the CFs with epoxy can be enhanced with the introduction of oxygen-containing groups at the interface.[2,5,12,15,58] Our results (see Figures 2 and 3) show that introducing CNC−CNT and CNC−GnP increases the oxygen-containing groups at the interface of CFRPs. Although these experiments suggest that hybrid NMs enhance the interactions of CF and epoxy, the formation of the interface and the mechanism of binding of hybrid NMs to the CF surface are still unraveled.

To understand the binding of hybrid NMs and CF sizing agents, we conduct low energy configuration DFT calculations. In this work, the sizing agent is composed of hydrophobic bisphenyl A and hydrophilic PEG groups with 10 repeated units (Figure S3) adopted from ref 53. The free binding energy of the CF sizing agent with CNC, CNC−GnP, and CNC−CNT with and without water is presented in Table 1. The higher free binding energy indicates a higher tendency to make bonds. The structures of CNC, water-CNT, and water-GnP with sizing molecules used in our computational study are displayed in Figure 6. To simulate the real conditions, the reference CNT and GnP are bonded to water molecules because their highly electropositive defected sites immediately react with water molecules in an aqueous suspension (see Figure 5). In the case of CNC-bonded CNT/GnP, the hypothesis is that water molecules are replaced with CNCs during ultrasonic treatment. Table 1 displays that the binding energy of the CNC sizing is 24.05 kcal/mol, where hydrogen bonds form between the PEG and hydroxyl groups of CNCs (Figure 6a). To understand the effect of the CNC presence in hybrid NMs, the binding energies of water-CNT/GnP-sizing (Figure 6b,c) are calculated. According to Table 1, the binding energy of water-CNT sizing is 51.74 kcal/mol, which is lower than that of CNC−CNT sizing (66.15 kcal/mol). This difference in binding energy indicates that the hybrid CNC−CNT creates stronger bonds with the CF sizing agent compared to that of water-CNT, which is in accordance with the previous study[69] that the addition of CNCs increases the binding energy of the system. A similar trend is observed for GnP in water, where the binding energy of water-GnP-sizing (47.61 kcal/mol) is lower than that of CNC−GnP-sizing (58.94 kcal/mol). These DFT calculations conclude that both hybrid CNC−CNT and CNC−GnP show higher binding energy to the sizing agent compared to those of individual CNC, CNT, and GnP. It is also reported that the binding energy of CNC−CNT with the sizing agent is 14% higher than that of CNC−GnP, which can be related to their shape effect, i.e., nanotube and nanosheet.

Table 1. Binding Energy of CNC, Water−CNT, CNC−CNT, Water−GnP, and CNC−GnP Combined with a Sizing Agent of CF Calculated by DFT

molecules	binding energy (kcal/mol)
CNC-sizing agent	24.05
Water−CNT-sizing agent	51.74
CNC−CNT-sizing agent	66.15
Water−GnP-sizing agent	47.61
CNC−GnP-sizing agent	58.94

To capture the difference in binding energies, we investigate the optimized structures (conformations) of CNC−CNT/GnP with the sizing agent as an output of low energy configuration calculations (Figure 7). In CNC−CNT, multiple interactions such as $\pi-\pi$ between CNT and the phenyl groups of the sizing as well as hydrogen bonding between CNC and the oxygen atoms of the PEG groups are created (Figure 7a). In CNC−GnP, CNC interacts with the PEG groups of the sizing; however, phenyl groups of the sizing have a distant and limited interaction with the GnP surface due to its sheet shape (Figure 7b). This leads to ∼14% weaker binding energy of CNC−GnP sizing (58.94 kcal/mol) compared to that of CNC−CNT sizing (66.15 kcal/mol).

DFT calculations show that the morphological differences result in 3D spatial flexibility of CNC−CNT, leading to a conformation that allows multiple interactions with the CF sizing molecule, including $\pi-\pi$ and hydrogen bonds (Figure 7a). Conversely, the 2D geometry of CNC−GnP limits its interaction with sizing molecules to hydrogen bonds (Figure 7b), which results in 14% lower binding energy. We conclude that the multiple interactions of CNC−CNT with the sizing agent due to the shape and 3D spatial flexibility of CNC−CNT is a contributing factor to enhance the interfacial properties of CFRP higher than that of CNC−GnP (see Figure 4b).

5. CONCLUSION

We explain the synergistic effect of hybrid CNC bonded-CNT/GnP on the formation of the interface, its chemical composition, and the mechanical properties of a hybrid CFRP composite for structural applications. We show that CNC provides a platform that enables engineering the chemical composition of the interface and its mechanical properties. We report a 200% rise in IFSS for 10:1 CNC−CNT-coated CFRP and 145% for 4:1 CNC−GnP-coated CFRP. Although both CNC−CNT and CNC−GnP enhance IFSS, ILSS, and tensile/flexural strength of composites, CNC−GnP improves tensile strength higher (by 33%) and CNC−CNT enhances the ILSS (by 46%) and flexural strength (by 55%) better in comparison to neat CFRPs. Our results show that introducing CNC−CNT/GnP on the CF surface increases the polar oxygen groups (C═O and C−O) at the CF/epoxy interface that promotes interfacial adhesion and creates a 4 μm interfacial region. In addition, the DFT calculations reveal that CNC−CNT has stronger free binding energy with the CF sizing compared to CNC−GnP. DFT results also reveal that

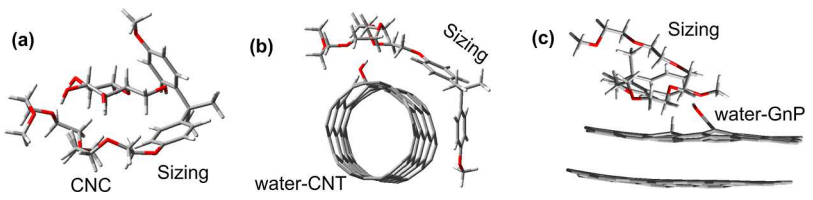

Figure 6. DFT models of (a) CNC−sizing, (b) water-CNT-sizing, and (c) water-GnP-sizing. The defected sites of CNT and GnP are saturated with water molecules.

https://doi.org/10.1021/acsanm.1c03860
ACS Appl. Nano Mater. 2022, 5, 1284−1295

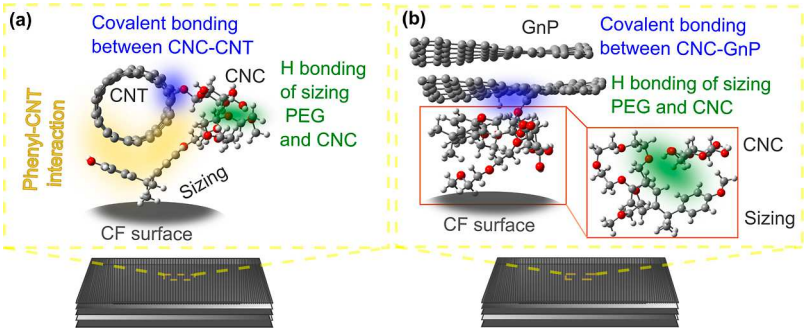

Figure 7. Optimized structures of (a) CNC−CNT and (b) CNC−GnP on the sizing agent of CF.

compared to the 2D geometry of CNC−GnP, the 3D spatial conformation of CNC−CNT creates multiple types of bonding with the sizing agent including hydrogen bonding and the $\pi-\pi$ interactions that result in higher binding energy. Our results layout the foundation to understand the mechanisms that form interfacial and interlaminar regions of hybrid nanostructured composites and provide a path forward to bottom-up manufacturing of composites with tailorable properties.

■ ASSOCIATED CONTENT

Supporting Information

The Supporting Information is available free of charge at https://pubs.acs.org/doi/10.1021/acsanm.1c03860.

SFF test sample, the sv of CNT and GnP models used in DFT, and sizing agent model used in DFT calculations (PDF)

The SI video compares the neat and CNC-CNT coated CFRPs during SFF test under optical microscope (MP4).

■ AUTHOR INFORMATION

Corresponding Author

Amir Asadi − *Department of Materials Science and Engineering and Department of Engineering Technology and Industrial Distribution, Texas A&M University, College Station, Texas 77843-3367, United States;* orcid.org/0000-0002-3174-362X; Phone: +1 (979)-458-7841; Email: amir.asadi@tamu.edu

Authors

Ozge Kaynan − *Department of Materials Science and Engineering, Texas A&M University, College Station, Texas 77843-3367, United States*

Lisa M. Pérez − *High Performance Research Computing, Texas A&M University, College Station, Texas 77843-3361, United States;* orcid.org/0000-0003-1176-1027

Complete contact information is available at: https://pubs.acs.org/10.1021/acsanm.1c03860

Notes

The authors declare no competing financial interest.

■ ACKNOWLEDGMENTS

This material is based upon work supported by the National Science Foundation under grant 1930277.

■ REFERENCES

(1) Asadi, A.; Miller, M.; Moon, R. J.; Kalaitzidou, K. Improving the interfacial and mechanical properties of short glass fiber/epoxy composites by coating the glass fibers with cellulose nanocrystals. *Express Polym. Lett.* **2016**, *10*, 587−597.

(2) Mahmood, H.; Vanzetti, L.; Bersani, M.; Pegoretti, A. Mechanical properties and strain monitoring of glass-epoxy composites with graphene-coated fibers. *Composites, Part A* **2018**, *107*, 112−123.

(3) Zhao, M.; Meng, L.; Ma, L.; Ma, L.; Yang, X.; Huang, Y.; Ryu, J. E.; Shankar, A.; Li, T.; Yan, C.; Guo, Z. Layer-by-layer grafting CNTs onto carbon fibers surface for enhancing the interfacial properties of epoxy resin composites. *Compos. Sci. Technol.* **2018**, *154*, 28−36.

(4) Ding, R.; Sun, Y.; Lee, J.; Nam, J.-D.; Suhr, J. Enhancing interfacial properties of carbon fiber reinforced epoxy composites by grafting MXene sheets (Ti2C). *Composites, Part B* **2021**, *207*, 108580.

(5) Wu, Q.; Bai, H.; Yang, X.; Zhu, J. Significantly increasing the interfacial adhesion of carbon fiber composites via constructing a synergistic hydrogen bonding network by vacuum filtration. *Composites, Part B* **2021**, *225*, 109300.

(6) Zhang, C.; Liu, L.; Xu, Z.; Lv, H.; Wu, N.; Zhou, B.; Mai, W.; Zhao, L.; Tian, X.; Guo, X. Improvement for interface adhesion of epoxy/carbon fibers endowed with carbon nanotubes via microwave plasma-enhanced chemical vapor deposition. *Polym. Compos.* **2018**, *39*, E1262−E1268.

(7) Qin, W.; Vautard, F.; Drzal, L. T.; Yu, J. Mechanical and electrical properties of carbon fiber composites with incorporation of graphene nanoplatelets at the fiber−matrix interphase. *Composites, Part B* **2015**, *69*, 335−341.

(8) Gangineni, P. K.; Yandrapu, S.; Ghosh, S. K.; Anand, A.; Prusty, R. K.; Ray, B. C. Mechanical behavior of Graphene decorated carbon fiber reinforced polymer composites: An assessment of the influence of functional groups. *Composites, Part A* **2019**, *122*, 36−44.

(9) Kaynan, O.; Atescan, Y.; Ozden-Yenigun, E.; Cebeci, H. Mixed Mode delamination in carbon nanotube/nanofiber interlayered composites. *Composites, Part B* **2018**, *154*, 186−194.

(10) Shariatnia, S.; Kumar, A. V.; Kaynan, O.; Asadi, A. Hybrid Cellulose Nanocrystal-Bonded Carbon Nanotubes/Carbon Fiber Polymer Composites for Structural Applications. *ACS Appl. Nano Mater.* **2020**, *3*, 5421−5436.

(11) Batista, M. D. R.; Drzal, L. T. Carbon fiber/epoxy matrix composite interphases modified with cellulose nanocrystals. *Compos. Sci. Technol.* **2018**, *164*, 274−281.

(12) Yao, X.; Gao, X.; Jiang, J.; Xu, C.; Deng, C.; Wang, J. Comparison of carbon nanotubes and graphene oxide coated carbon fiber for improving the interfacial properties of carbon fiber/epoxy composites. *Composites, Part B* **2018**, *132*, 170−177.

(13) Yuan, X.; Zhu, B.; Cai, X.; Qiao, K.; Zhao, S.; Zhang, M.; Yu, J. Micro-configuration controlled interfacial adhesion by grafting graphene oxide onto carbon fibers. *Composites, Part A* **2018**, *111*, 83−93.

(14) Kim, S.-H.; Park, S.-J. Effect of graphene oxide/graphitic nanofiber nanohybrids on interfacial properties and fracture tough-

ness of carbon fibers-reinforced epoxy matrix composites. *Composites, Part B* **2021**, *227*, 109387.
(15) Kwon, Y. J.; Kim, Y.; Jeon, H.; Cho, S.; Lee, W.; Lee, J. U. Graphene/carbon nanotube hybrid as a multi-functional interfacial reinforcement for carbon fiber-reinforced composites. *Composites, Part B* **2017**, *122*, 23−30.
(16) Tamrakar, S.; An, Q.; Thostenson, E. T.; Rider, A. N.; Haque, B. Z.; Gillespie, J. W., Jr Tailoring interfacial properties by controlling carbon nanotube coating thickness on glass fibers using electrophoretic deposition. *ACS Appl. Mater. Interfaces* **2016**, *8*, 1501−1510.
(17) Kumar, A.; Shariatnia, S.; Asadi, A. *In Cellulose Nanocrystals Assisted Process to Integrate Carbon Nanotubes in CFRP Composites*; AIAA Scitech 2020 Forum, 2020; p 0155.
(18) Liu, L.; Yan, F.; Li, M.; Zhang, M.; Xiao, L.; Shang, L.; Ao, Y. Improving interfacial properties of hierarchical reinforcement carbon fibers modified by graphene oxide with different bonding types. *Composites, Part A* **2018**, *107*, 616−625.
(19) Zhang, W.; Deng, X.; Sui, G.; Yang, X. Improving interfacial and mechanical properties of carbon nanotube-sized carbon fiber/epoxy composites. *Carbon* **2019**, *145*, 629−639.
(20) Zhang, X.; Fan, X.; Yan, C.; Li, H.; Zhu, Y.; Li, X.; Yu, L. Interfacial microstructure and properties of carbon fiber composites modified with graphene oxide. *ACS Appl. Mater. Interfaces* **2012**, *4*, 1543−1552.
(21) Hamedi, M. M.; Hajian, A.; Fall, A. B.; Håkansson, K.; Salajkova, M.; Lundell, F.; Wågberg, L.; Berglund, L. A. Highly conducting, strong nanocomposites based on nanocellulose-assisted aqueous dispersions of single-wall carbon nanotubes. *ACS Nano* **2014**, *8*, 2467−2476.
(22) Qin, W.; Chen, C.; Zhou, J.; Meng, J. Synergistic effects of graphene/carbon nanotubes hybrid coating on the interfacial and mechanical properties of fiber composites. *Materials* **2020**, *13*, 1457.
(23) Bekyarova, E.; Thostenson, E. T.; Yu, A.; Kim, H.; Gao, J.; Tang, J.; Hahn, H. T.; Chou, T.-W.; Itkis, M. E.; Haddon, R. C. Multiscale carbon nanotube− carbon fiber reinforcement for advanced epoxy composites. *Langmuir* **2007**, *23*, 3970−3974.
(24) Davis, D. C.; Wilkerson, J. W.; Zhu, J.; Hadjiev, V. G. A strategy for improving mechanical properties of a fiber reinforced epoxy composite using functionalized carbon nanotubes. *Compos. Sci. Technol.* **2011**, *71*, 1089−1097.
(25) Kundalwal, S. I.; Ray, M. C. Effect of carbon nanotube waviness on the effective thermoelastic properties of a novel continuous fuzzy fiber reinforced composite. *Composites, Part B* **2014**, *57*, 199−209.
(26) Li, N.; Li, Y.; Zhou, J.; He, Y.; Hao, X. Drilling delamination and thermal damage of carbon nanotube/carbon fiber reinforced epoxy composites processed by microwave curing. *Int. J. Mach. Tool Manufact.* **2015**, *97*, 11−17.
(27) Tehrani, M.; Boroujeni, A. Y.; Hartman, T. B.; Haugh, T. P.; Case, S. W.; Al-Haik, M. S. Mechanical characterization and impact damage assessment of a woven carbon fiber reinforced carbon nanotube−epoxy composite. *Compos. Sci. Technol.* **2013**, *75*, 42−48.
(28) Thostenson, E. T.; Li, W. Z.; Wang, D. Z.; Ren, Z. F.; Chou, T. W. Carbon nanotube/carbon fiber hybrid multiscale composites. *J. Appl. Phys.* **2002**, *91*, 6034−6037.
(29) Zhou, H. W.; Mishnaevsky, L., Jr; Yi, H. Y.; Liu, Y. Q.; Hu, X.; Warrier, A.; Dai, G. M. Carbon fiber/carbon nanotube reinforced hierarchical composites: Effect of CNT distribution on shearing strength. *Composites, Part B* **2016**, *88*, 201−211.
(30) Gao, B.; Zhang, R.; He, M.; Sun, L.; Wang, C.; Liu, L.; Zhao, L.; Cui, H.; Cao, A. Effect of a multiscale reinforcement by carbon fiber surface treatment with graphene oxide/carbon nanotubes on the mechanical properties of reinforced carbon/carbon composites. *Composites, Part A* **2016**, *90*, 433−440.
(31) Kong, Q.-Q.; Liu, Z.; Gao, J.-G.; Chen, C.-M.; Zhang, Q.; Zhou, G.; Tao, Z.-C.; Zhang, X.-H.; Wang, M.-Z.; Li, F.; Cai, R. Hierarchical graphene−carbon fiber composite paper as a flexible lateral heat spreader. *Adv. Funct. Mater.* **2014**, *24*, 4222−4228.
(32) Zhang, X.; Yang, W.; Zhang, J.; Ge, X.; Liu, X.; Zhan, Y. Multiscale graphene/carbon fiber reinforced copper matrix hybrid composites: Microstructure and properties. *Mater. Sci. Eng. A* **2019**, *743*, 512−519.
(33) Song, N.; Gao, Z.; Li, X. Tailoring nanocomposite interfaces with graphene to achieve high strength and toughness. *Sci. Adv.* **2020**, *6*, No. eaba7016.
(34) Sritharan, R.; Askari, D. Enhancing the short-beam strength of composite laminates using helical carbon nanotubes. *Composites, Part B* **2021**, *221*, 108999.
(35) Moon, R. J.; Martini, A.; Nairn, J.; Simonsen, J.; Youngblood, J. Cellulose nanomaterials review: structure, properties and nanocomposites. *Chem. Soc. Rev.* **2011**, *40*, 3941−3994.
(36) Löbmann, K.; Wohlert, J.; Müllertz, A.; Wågberg, L.; Svagan, A. J. Cellulose Nanopaper and Nanofoam for Patient-Tailored Drug Delivery. *Adv. Mater. Interfac.* **2017**, *4*, 1600655.
(37) Zhao, D.; Zhu, Y.; Cheng, W.; Chen, W.; Wu, Y.; Yu, H. Cellulose-based flexible functional materials for emerging intelligent electronics. *Adv. Mater.* **2021**, *33*, 2000619.
(38) Bhatnagar, A.; Sain, M. Processing of cellulose nanofiber-reinforced composites. *J. Reinforc. Plast. Compos.* **2005**, *24*, 1259−1268.
(39) de Souza, G.; Tarpani, J. R. Spraycoating of Nanocellulose Fibrilated (CNF) onto Glass Fiber and Carbon Fiber Fabrics and its Role as Hierarchical Reinforcement on GFRP and CFRP composites. *Compos. Interfac.* **2021**, 1−20.
(40) Dorigato, A.; Morandi, S.; Pegoretti, A. Effect of nanoclay addition on the fiber/matrix adhesion in epoxy/glass composites. *J. Compos. Mater.* **2012**, *46*, 1439−1451.
(41) Gao, S.; Mader, E.; Plonka, R. Nanocomposite coatings for healing surface defects of glass fibers and improving interfacial adhesion. *Compos. Sci. Technol.* **2008**, *68*, 2892−2901.
(42) Pedrazzoli, D.; Pegoretti, A.; Kalaitzidou, K. Synergistic effect of exfoliated graphite nanoplatelets and short glass fiber on the mechanical and interfacial properties of epoxy composites. *Compos. Sci. Technol.* **2014**, *98*, 15−21.
(43) Szabó, L.; Imanishi, S.; Hirose, D.; Tsukegi, T.; Wada, N.; Takahashi, K. Mussel-Inspired Design of a Carbon Fiber−Cellulosic Polymer Interface toward Engineered Biobased Carbon Fiber-Reinforced Composites. *ACS Omega* **2020**, *5*, 27072−27082.
(44) Uribe, B. E. B.; Chiromito, E. M. S.; Carvalho, A. J. F.; Tarpani, J. R. Low-cost, environmentally friendly route for producing CFRP laminates with microfibrillated cellulose interphase. *Express Polym. Lett.* **2017**, *11*, 47.
(45) Batmaz, R.; Mohammed, N.; Zaman, M.; Minhas, G.; Berry, R. M.; Tam, K. C. Cellulose nanocrystals as promising adsorbents for the removal of cationic dyes. *Cellulose* **2014**, *21*, 1655−1665.
(46) Foster, E. J.; Moon, R. J.; Agarwal, U. P.; Bortner, M. J.; Bras, J.; Camarero-Espinosa, S.; Chan, K. J.; Clift, M. J. D.; Cranston, E. D.; Eichhorn, S. J.; Fox, D. M.; Hamad, W. Y.; Heux, L.; Jean, B.; Korey, M.; Nieh, W.; Ong, K. J.; Reid, M. S.; Renneckar, S.; Roberts, R.; Shatkin, J. A.; Simonsen, J.; Stinson-Bagby, K.; Wanasekara, N.; Youngblood, J. Current characterization methods for cellulose nanomaterials. *Chem. Soc. Rev.* **2018**, *47*, 2609−2679.
(47) Miyashiro, D.; Hamano, R.; Umemura, K. A review of applications using mixed materials of cellulose, nanocellulose and carbon nanotubes. *Nanomaterials* **2020**, *10*, 186.
(48) Sager, R.; Klein, P.; Lagoudas, D.; Zhang, Q.; Liu, J.; Dai, L.; Baur, J. Effect of carbon nanotubes on the interfacial shear strength of T650 carbon fiber in an epoxy matrix. *Compos. Sci. Technol.* **2009**, *69*, 898−904.
(49) Kelly, A.; Tyson, W. R. Tensile properties of fibre-reinforced metals: copper/tungsten and copper/molybdenum. *J. Mech. Phys. Solid.* **1965**, *13*, 329−350.
(50) Becke, A. D. Density-functional exchange-energy approximation with correct asymptotic behavior. *Phys. Rev.* **1988**, *38*, 3098.
(51) Ditchfield, R.; Hehre, W. J.; Pople, J. A. Self-consistent molecular-orbital methods. IX. An extended Gaussian-type basis for molecular-orbital studies of organic molecules. *J. Chem. Phys.* **1971**, *54*, 724−728.

https://doi.org/10.1021/acsanm.1c03860
ACS Appl. Nano Mater. 2022, 5, 1284−1295

(52) Marenich, A. V.; Cramer, C. J.; Truhlar, D. G. Universal solvation model based on solute electron density and on a continuum model of the solvent defined by the bulk dielectric constant and atomic surface tensions. *J. Phys. Chem. B* **2009**, *113*, 6378−6396.
(53) Asai, H.; Anai, K. Method of sizing carbon fiber and a carbon fiber composition. WO 2016193927 A1, 1987.
(54) Hajian, A.; Lindström, S. B.; Pettersson, T.; Hamedi, M. M.; Wågberg, L. Understanding the dispersive action of nanocellulose for carbon nanomaterials. *Nano Lett.* **2017**, *17*, 1439−1447.
(55) Liu, Y.; Sun, B.; Li, J.; Cheng, D.; An, X.; Yang, B.; He, Z.; Lutes, R.; Khan, A.; Ni, Y. Aqueous dispersion of carbon fibers and expanded graphite stabilized from the addition of cellulose nanocrystals to produce highly conductive cellulose composites. *ACS Sustainable Chem. Eng.* **2018**, *6*, 3291−3298.
(56) Chen, J.; Zhao, D.; Jin, X.; Wang, C.; Wang, D.; Ge, H. Modifying glass fibers with graphene oxide: towards high-performance polymer composites. *Compos. Sci. Technol.* **2014**, *97*, 41−45.
(57) Sun, L.; Li, M.; Shang, L.; Xiao, L.; Liu, Y.; Zhang, M.; Ao, Y. The influence of oxygen on skin-core structure of polyacrylonitrile-based precursor fibers. *Polymer* **2020**, *197*, 122516.
(58) Srivastava, A. K.; Gupta, V.; Yerramalli, C. S.; Singh, A. Flexural strength enhancement in carbon-fiber epoxy composites through graphene nano-platelets coating on fibers. *Composites, Part B* **2019**, *179*, 107539.
(59) Yao, H.; Sui, X.; Zhao, Z.; Xu, Z.; Chen, L.; Deng, H.; Liu, Y.; Qian, X. Optimization of interfacial microstructure and mechanical properties of carbon fiber/epoxy composites via carbon nanotube sizing. *Appl. Surf. Sci.* **2015**, *347*, 583−590.
(60) Chen, L.; Jin, H.; Xu, Z.; Shan, M.; Tian, X.; Yang, C.; Wang, Z.; Cheng, B. A design of gradient interphase reinforced by silanized graphene oxide and its effect on carbon fiber/epoxy interface. *Mater. Chem. Phys.* **2014**, *145*, 186−196.
(61) Lu, K.; Zhu, W.; Su, Q.; Li, G.; Yang, X. Correlation between compression strength and failure mechanism of carbon fiber composite with tailored modulus of amide acid/SiO2 synergistically stiffened epoxy matrix. *Compos. Sci. Technol.* **2021**, *202*, 108593.
(62) Yan, M.; Liu, L.; Chen, L.; Li, N.; Jiang, Y.; Xu, Z.; Jing, M.; Hu, Y.; Liu, L.; Zhang, X. Radiation resistance of carbon fiber-reinforced epoxy composites optimized synergistically by carbon nanotubes in interface area/matrix. *Composites, Part B* **2019**, *172*, 447−457.
(63) Zhao, Z.; Teng, K.; Li, N.; Li, X.; Xu, Z.; Chen, L.; Niu, J.; Fu, H.; Zhao, L.; Liu, Y. Mechanical, thermal and interfacial performances of carbon fiber reinforced composites flavored by carbon nanotube in matrix/interface. *Compos. Struct.* **2017**, *159*, 761−772.
(64) Sui, X.; Shi, J.; Yao, H.; Xu, Z.; Chen, L.; Li, X.; Ma, M.; Kuang, L.; Fu, H.; Deng, H. Interfacial and fatigue-resistant synergetic enhancement of carbon fiber/epoxy hierarchical composites via an electrophoresis deposited carbon nanotube-toughened transition layer. *Composites, Part A* **2017**, *92*, 134−144.
(65) Chen, L.; Jin, H.; Xu, Z.; Li, J.; Guo, Q.; Shan, M.; Yang, C.; Wang, Z.; Mai, W.; Cheng, B. Role of a gradient interface layer in interfacial enhancement of carbon fiber/epoxy hierarchical composites. *J. Mater. Sci.* **2015**, *50*, 112−121.
(66) Zhang, C.; Pei, X.; Xu, Z.; Wang, C.; Zhang, G.; Guo, X.; Fu, H.; Wu, N. Performance of composites via multiple interface engineering techniques: plasma etching, UV-induced grafting and nanotube deposition. *Mater. Today Commun.* **2020**, *22*, 100723.
(67) Kumar, S.; Graninger, G.; Hawkins, S. C.; Falzon, B. G. A nanostructured cellulose-based interphase layer to enhance the mechanical performance of glass fibre-reinforced polymer composites. *Composites, Part A* **2021**, *148*, 106475.
(68) Juntaro, J.; Pommet, M.; Mantalaris, A.; Shaffer, M.; Bismarck, A. Nanocellulose enhanced interfaces in truly green unidirectional fibre reinforced composites. *Compos. Interfac.* **2007**, *14*, 753−762.
(69) Shishehbor, M.; Pouranian, M. R. Tuning the Mechanical and Adhesion Properties of Carbon Nanotubes Using Aligned Cellulose Wrap (Cellulose Nanotube): A Molecular Dynamics Study. *Nanomaterials* **2020**, *10*, 154.
(70) Shishehbor, M.; Dri, F. L.; Moon, R. J.; Zavattieri, P. D. A continuum-based structural modeling approach for cellulose nanocrystals (CNCs). *J. Mech. Phys. Solid.* **2018**, *111*, 308−332.
(71) Lu, A. J.; Pan, B. C. Nature of single vacancy in achiral carbon nanotubes. *Phys. Rev. Lett.* **2004**, *92*, 105504.
(72) El-Barbary, A. A.; Telling, R. H.; Ewels, C. P.; Heggie, M. I.; Briddon, P. R. Structure and energetics of the vacancy in graphite. *Phys. Rev. B: Condens. Matter Mater. Phys.* **2003**, *68*, 144107.

https://doi.org/10.1021/acsanm.1c03860
ACS Appl. Nano Mater. 2022, 5, 1284−1295